**53rd AIAA/ASME/ASCE/AHS/ASC Structures, Structural Dynamics and Materials Conference
20th AI**
23 - 26 April 2012, Honolulu, Hawaii

AIAA 2012-1401

Intrinsic models for nonlinear flexible-aircraft dynamics using industrial finite-element and loads packages

Rafael Palacios[*], Yinan Wang[†]

Imperial College, London SW7 2AZ, United Kingdom

Moti Karpel[‡]

Technion - Israel Institute of Technology, Haifa 32000, Israel

A procedure is introduced to construct 1-D geometrically-nonlinear structural dynamics models from built-up 3-D finite-element solutions. The nonlinear 1-D model is based on an intrinsic form of the equations of motion, that uses beam velocities and internal forces as primary degrees of freedom. It is further written in modal form, which yields a description of the beam dynamics through ordinary differential equations with quadratic non-linearities. We show that the evaluation of the coefficients in these nonlinear equations of motion does not require the generation of a beam finite-element model. Instead, they are directly identified in the 3-D model through a process of static condensation of the dynamics on nodes defined along along spanwise stations, as it is done in aircraft dynamic load analysis. In fact, the method exploits the multi-point constraints of linear load models, that are normally used to obtain sectional loads, and we show how it can be integrated in full-vehicle aeroelastic analysis. Finally we illustrate this approach on an isotropic cantilever box beam modelled using shell elements.

Nomenclature

$\mathbf{c}(s)$	cross-sectional compliance matrix
$\mathbf{F}(s,t)$	Beam internal forces in material coordinates
$\mathbf{f}_1(s,t)$	Applied forces/moments per unit length
$\mathbf{V}(s,t)$	Beam translational velocities in material coordinates
$\mathbf{K}_a$	Stiffness matrix in reduced set of FE problem
$\mathbf{M}(s,t)$	Beam internal moments in material coordinates
$\mathbf{M}_a$	Mass matrix in reduced set of FE problem
$\mathbf{m}(s)$	cross-sectional mass matrix
$q_1(t)$	intrinsic modal coordinates (velocity component)
$q_2(t)$	intrinsic modal coordinates (internal force component)
s	curvilinear coordinate along reference line
t	time
$\mathbf{x}_1(s,t)$	local velocities state vector
$\mathbf{x}_2(s,t)$	internal force/moment state vector
$\mathbf{\Phi}_j(s)$	Mode shape j in intrinsic degree of freedom (velocities/forces)
ϕ_{aj}	Discrete mode shape j in reduced set of FE problem
$\mathbf{\Omega}(s,t)$	Beam rotational velocities in material coordinates
ω_j	Natural frequency of mode j

---

[*]Lecturer, Department of Aeronautics, AIAA Member
[†]Graduate student, Department of Aeronautics
[‡]Sanford Kaplan Chair Professor, Faculty of Aerospace Engineering, AIAA Fellow

American Institute of Aeronautics and Astronautics

I.   Introduction

The aeroelastic analysis of the new generation of very-long-endurance UAVs, with flexible high-aspect-ratio wings, requires efficient computational models that are able to account for geometrically-nonlinear structural effects. They are not captured by the standard linear methods based on the natural vibration modes of the structure, and the common approach for over a decade has been to construct purpose-built models *from scratch* with nonlinear beam elements and lifting-line aerodynamics.[1–5] While this approach has provided substantial insight into the dynamic response of Very Flexible Aircraft (VFA), including the coupling with the flight dynamics, it is also based on a vehicle representation of much lower fidelity than the (linear) aeroelastic tools commonly used in industrial applications (e.g., NASTRAN or ZAERO). Firstly, unsteady aerodynamics based on 2-D Theodorsen-type modelling does not include spanwise aerodynamic interference, interaction between different aerodynamic surfaces, or the effect of bodies, as the doublet-lattice method (DLM) does. This can be overcome –for the case of large wing displacements– by using generic time-domain panel methods, such as the the unsteady vortex-lattice method (UVLM).[6] It uses the same level of fidelity, and indeed the same panel discretization on the lifting surfaces, of the DLM while accounting for the actual wing kinematics. UVLM solutions are available either in time-marching solutions[7,8] or in discrete state-space form[9] (A pending problem is, however, the ability to capture wing stall in the dynamic response to gust or other load events, but this issue is common to all methodologies based on potential flow theory).

A second compromise on the existing nonlinear VFA models is the fidelity of the beam-based structural dynamics model. While substantial effort has been done in the development of geometrically-exact composite beam theories and their integration into full-vehicle modelling, the constitutive relations (i.e., the matrices of mass and stiffness per unit length) are based on either estimates of section moments of inertia or purpose-built homogenisation tools based on either cross-sectional[10] or unit-cell[11] analysis. However, none of those procedures currently links to the actual detailed 3-D finite-element (FEM) model of the vehicle which are built, and refined, during several loops in the load design cycle.

A basic question that remains to be answered is then how the nonlinear analysis of flexible aircraft dynamics, which have so far been carried out at the *conceptual design* level can be adopted in subsequent stages of the design cycle. A common view, is that the mismatch between the (nonlinear) composite beam models for *conceptual design* and the built-up (linear) 3-D FE models routinely used by aircraft designers in industrial setting is indeed very large. However, there are several practical aspects that bring 3-D FE results much closer to a beam description in typical dynamic loads and aeroelastic analysis on (needless to say) high-aspect-ratio-wing aircraft:

- Firstly, the low-frequency vibration modes are indeed bending (in-plane or out-of-plane) and torsion modes. This is clearly a beam concept;

- Secondly, wing loads are evaluated in terms of resultant forces and moments (another beam concept) at varying locations, commonly known as *monitoring stations*, along the wing span.

- A final consideration is that production models for dynamic loads and aeroelasticity often use lumped masses to model inertia, and those are located along the longitudinal axes of wings, fuselage and tail (although also at the engines, landing gear, etc.). The nodes where they are located become the basis for static condensation of the equations before the evaluation of natural modes.

If a linear beam model (a *stick model*) of the vehicle were to provide a good approximation to the low-frequency modes *and* a good estimation of the dynamic loads at the monitoring stations, then one could safely replace the original model by the beam equivalent. Indeed such *stick models* have long been used in aeroelastic design and provide good accuracy that for large enough wing aspect ratios.[12] The obvious next step is to use geometrically-nonlinear extensions of those beam models to study dynamic loads with large wing excursions. Those beam models are clearly more tractable for nonlinear analysis that direct use of the original 3-D FEM model, but they still have much higher complexity than the linear modal equations. To overcome this, this paper will show a procedure by which the fidelity of the original 3-D linear FEM model is preserved (indeed it uses directly its "exact" linear modes) while introducing the non-linearities as higher-order corrections on a particular description of the modal equations of motion.

The first step will be to identify a suitable nonlinear composite beam theory. Among the myriad of solutions in the literature, intrinsic formulations[13,14] will be particularly useful to our goals. An intrinsic beam theory draws from Kirchhoff's analogy between the spatial and time derivatives[15] to define a two-field

American Institute of Aeronautics and Astronautics

description of the beam dynamics on first-derivatives, i.e., strains and velocities. This results in a formulation that closely resembles that of rigid-body dynamics, with first order equations of motion in both beam strains and velocities and, critically for the goals of this paper, only quadratic non-linearities on those primary states. As in rigid-body dynamics, the solution process is closed by the propagation equations to obtain displacement and rotations. The transcendental non-linearities associated to the finite rotations are then transferred to that post-processing step (which may be even skipped in many problems in aeroelasticity).[16]

Previous work by the first author[17] has the nonlinear vibrations of composite beams using a nonlinear intrinsic formulation. Following on that work, this paper will investigate the generation of the equations of motion in intrinsic modal coordinates from built-up 3-D FEM models. The starting point is the assumption that such a 3-D model of the structure already exists and provides the bases for dynamic load and aeroelastic analysis based on linear methods. This FEM model is then reduced using static condensation[18, 19] (Guyan reduction) to a small set of grid points along the aircraft *beam skeleton*, those displacements are obtained from averaging the local degrees of freedom (RBE3 constraints in NASTRAN). The selection of that *skeleton* is therefore critical, but it can be done with the same criteria as the monitoring stations where dynamic loads are evaluated. More sophisticated methods of dynamic condensation are available in the literature[20] and they could be equally considered within the proposed approach. However, Guyan reduction is the most common method for dynamic load analysis and it is readily available in most finite-element packages, so it was preferred here. The mode shapes of the full 3-D model on the set of beam nodes will be used to defined directly the linear part of the equation. Identification of the equivalent beam local stiffness and inertia can then be carried out to obtain the nonlinear terms of the equations of motion in intrinsic modal coordinates.

II. Modelling Aspects

The intrinsic equations of motion for a geometrically-nonlinear composite beam are described first, followed by a projection of the equations into a modal space and the description of how those modal equations are integrated in vehicle analysis.

A. Intrinsic Beam Model

Following Cosserat's model, a beam will be defined as a solid determined by the rigid motion of cross sections linked to a deformable reference line, Γ. There are no assumptions on the sectional material or geometric properties, other than the condition of slenderness. Let s be the arc length, $\mathbf{V}(s,t)$ and $\mathbf{\Omega}(s,t)$ the instantaneous translational and angular inertial velocities, and $\mathbf{F}(s,t)$ and $\mathbf{M}(s,t)$ the sectional internal forces and moments along the reference line. All these vectors are expressed in their components in the local (deformed) material frame. Using this magnitudes, Hodges has[14] derived the intrinsic form of the beam equations, which are written here as[16, 17]

$$\mathbf{m}\dot{\mathbf{x}}_1 - \mathbf{x}_2' - \mathbf{e}\mathbf{x}_2 + \mathcal{L}_1(\mathbf{x}_1)\mathbf{m}\mathbf{x}_1 + \mathcal{L}_2(\mathbf{x}_2)\mathbf{c}\mathbf{x}_2 = \mathbf{f}_1,$$
$$\mathbf{c}\dot{\mathbf{x}}_2 - \mathbf{x}_1' + \mathbf{e}^\top\mathbf{x}_1 - \mathcal{L}_1^\top(\mathbf{x}_1)\mathbf{c}\mathbf{x}_2 = \mathbf{0},$$

(1)

where dots and primes denote derivatives with time, t, and the arc length, s, respectively. The first equation is the actual equation of motion, while the second is a kinematic compatibility condition. The state vectors $\mathbf{x}_1$ and $\mathbf{x}_2$ and the force vector $\mathbf{f}_1$ are given by

$$\mathbf{x}_1 = \left\{ \begin{array}{c} \mathbf{V} \\ \mathbf{\Omega} \end{array} \right\}, \quad \mathbf{x}_2 = \left\{ \begin{array}{c} \mathbf{F} \\ \mathbf{M} \end{array} \right\}, \quad \text{and} \quad \mathbf{f}_1 = \left\{ \begin{array}{c} f_a \\ m_a \end{array} \right\}.$$

(2)

The constant matrix $\mathbf{e}$ and the linear matrix operators $\mathcal{L}_1$ and $\mathcal{L}_2$ are

$$\mathbf{e} = \left[\begin{array}{cc} 0 & 0 \\ \tilde{\mathbf{e}}_1 & 0 \end{array} \right], \quad \mathcal{L}_1(\mathbf{x}_1) = \left[\begin{array}{cc} \tilde{\mathbf{\Omega}} & 0 \\ \tilde{\mathbf{V}} & \tilde{\mathbf{\Omega}} \end{array} \right], \quad \text{and} \quad \mathcal{L}_2(\mathbf{x}_2) = \left[\begin{array}{cc} 0 & \tilde{\mathbf{F}} \\ \tilde{\mathbf{F}} & \tilde{\mathbf{M}} \end{array} \right].$$

(3)

where $\tilde{\bullet}$ is the skew-symmetric (or cross-product) operator and $\mathbf{e}_1 = \{1, 0, 0\}^\top$. As this is a beam model, the only necessary coefficients in the equations are the matrices of mass, $\mathbf{m}$, and compliance, $\mathbf{c}$, per unit length, which are full but symmetric matrices. Eqs. (1) need to be solved with a set of boundary and initial conditions, which are also written in terms of velocities and forces.[14]

Displacements and rotations are dependent variables, which only appear explicitly if the applied forces and moments, $\mathbf{f}_1$, depend on them. They are obtained either from time integration of the inertial velocities, as in rigid-body dynamics;[21] or from spatial integration of the internal forces and moments (strains),[22, 23] as with the Frenet-Serret formulae in differential geometry.

B.   Nonlinear Equations in Intrinsic Modal Coordinates

The linear normal modes (LNMs) are obtained first from the linearisation of the unforced (homogeneous) equations around a static equilibrium condition (i.e., $\mathbf{x}_1(s,0) = 0$ and $\mathbf{x}_2(s,0) = \hat{\mathbf{x}}_2(s)$). The LNMs are obtained in the usual way, as the non-trivial solutions of this homogeneous equation that satisfy the spatial boundary conditions.

To simplify the argumentation in this paper, it will be assumed that the reference line Γ is an open kinematic chain (it has no closed loops) with constant properties, that is, matrices $\mathbf{m}$ and $\mathbf{c}$ are constant, and that the LNMs are obtained about the undeformed configuration (i.e. $\hat{\mathbf{x}}_2 = 0$). There is a more general version of this theory that does not require those assumptions, but it will not be discussed here. Under those assumptions, the LNMs in the intrinsic degrees of freedom, $\mathbf{\Phi}_j(s)$, are obtained as[17]

$$\mathbf{\Phi}_j(s) = e^{\mathbf{A}(\omega_j)s}\mathbf{\Phi}_j(0), \tag{4}$$

with

$$\mathbf{\Phi}_j = \left\{ \begin{array}{c} \mathbf{\Phi}_{1j} \\ \mathbf{\Phi}_{2j} \end{array} \right\} \quad \text{and} \quad \mathbf{A}(\omega_j) = \left[\begin{array}{cc} \mathbf{e}^\top & -\omega_j\mathbf{c} \\ \omega_j\mathbf{m} & -\mathbf{e} \end{array} \right], \tag{5}$$

and where ω_j are the natural angular frequencies and $\mathbf{\Phi}_{1j}(s)$ and $\mathbf{\Phi}_{2j}(s)$ the components of the mode shapes in terms of linear/angular velocities and internal forces/moments, respectively. $\mathbf{\Phi}_j(0)$ are the values of the eigenmodes at the origin for arc lengths ($s = 0$), which are obtained, except for a normalization constant, by enforcing the boundary conditions. Modes are normalized as

$$\int_\Gamma \mathbf{\Phi}_{1j}^\top \mathbf{m}\mathbf{\Phi}_{1k}ds = \delta_{jk},$$
$$\int_\Gamma \mathbf{\Phi}_{2j}^\top \mathbf{c}\mathbf{\Phi}_{2k}ds = \delta_{jk}. \tag{6}$$

The previous conditions are actually redundant and only one of them needs to be enforced to normalize the mode shapes in intrinsic coordinates. This property will be used later in the identification of the modes from 3-D FEM. The modal expansions will be then defined as

$$\mathbf{x}_1(s,t) = \mathbf{\Phi}_{1j}(s)q_{1j}(t),$$
$$\mathbf{x}_2(s,t) = \mathbf{\Phi}_{2j}(s)q_{2j}(t), \tag{7}$$

where (q_{1j}, q_{2j}) are pairs of *intrinsic modal coordinates*. Note that we use Einstein notation to sum over repeated indices. Since this is a first-order theory, each natural frequency will be associated to two generalized coordinates. This approximation is used now to project Eqs. (1). By substituting Eq. (7) into that equation, and after using orthogonality conditions on the mode shapes, one obtains the equations of motion in intrinsic modal coordinates, as

$$\dot{q}_{1j} = \quad \omega_j q_{2j} - \beta_1^{jkl}q_{1k}q_{1l} - \beta_2^{jkl}q_{2k}q_{2l} + Q_{1j},$$
$$\dot{q}_{2j} = -\omega_j q_{1j} + \beta_2^{kjl}q_{1k}q_{2l}, \tag{8}$$

with $Q_{1j} = \int_\Gamma \mathbf{\Phi}_{1j}^\top \mathbf{f}_1 ds$ and

$$\beta_1^{jkl} = \int_\Gamma \mathbf{\Phi}_{1j}^\top \mathcal{L}_1\left(\mathbf{\Phi}_{1k}\right)\mathbf{m}\mathbf{\Phi}_{1l}ds,$$
$$\beta_2^{jkl} = \int_\Gamma \mathbf{\Phi}_{1j}^\top \mathcal{L}_2\left(\mathbf{\Phi}_{2k}\right)\mathbf{c}\mathbf{\Phi}_{2l}ds. \tag{9}$$

Note that the first order linear equations correspond to the Hamiltonian form of a single degree of freedom oscillator. The quadratic terms are obtained from the mode shapes and the mass and compliance matrices. This is the only information required to construct a geometrically-nonlinear description of the problem. As we will show below, that information can be extracted directly from a built-up 3-D FE model of the actual configuration.

American Institute of Aeronautics and Astronautics

C.   Relation with displacement/rotation degrees of freedom

A full description of the beam dynamics has been obtained without any need of the actual position vector and local orientation of the reference line (provided, as mentioned above, that the applied forces do not depend on that information). Those can be found for the general nonlinear case elsewhere,[14, 23] but they will be introduced here only for the linear problem. For that purpose, we define now a new state vector

$$\mathbf{x}_0 = \left\{ \begin{array}{c} \mathbf{u} \\ \boldsymbol{\theta} \end{array} \right\}, \quad \text{such that } \dot{\mathbf{x}}_0 = \mathbf{x}_1, \tag{10}$$

and we will identify the components of this vector as the linear displacement, $\mathbf{R}(s,t)$, and linear rotation, $\boldsymbol{\theta}(s,t)$, respectively. Note that this has been presented as a definition, but one that yields the usual beam kinematics description in the linear approximation. Consider now the small-amplitude free vibrations of the structure, that is, the problem with $Q_{1j} = 0$ and $\beta = 0$ in Eq. (8). Solving that problem, and after recovering the original degrees of freedom through Eq. (7), yields

$$\begin{aligned} \mathbf{x}_1^{lin} &= \alpha_j \boldsymbol{\Phi}_{1j} \sin\left(\omega_j t + \varphi_j\right), \\ \mathbf{x}_2^{lin} &= \alpha_j \boldsymbol{\Phi}_{2j} \cos\left(\omega_j t + \varphi_j\right). \end{aligned} \tag{11}$$

where α_j and φ_j are real constants that depend on the initial conditions. This can be also be written in terms of the state vector (10). Assume $\boldsymbol{\Phi}_{0j}(s)$ is the displacement/rotation description of the mode shape associated to eigenvalue ω_j. It will be

$$\begin{aligned} \mathbf{x}_0^{lin} &= \alpha_j' \boldsymbol{\Phi}_{0j} \cos\left(\omega_j t + \varphi_j\right), \\ \mathbf{x}_1^{lin} &= -\alpha_j' \omega_j \boldsymbol{\Phi}_{0j} \sin\left(\omega_j t + \varphi_j\right), \\ \mathbf{x}_2^{lin} &= -\alpha_j' \mathbf{c}^{-1} \left(\boldsymbol{\Phi}_{0j}' - \mathbf{e}^\top \boldsymbol{\Phi}_{0j}\right) \cos\left(\omega_j t + \varphi_j\right). \end{aligned} \tag{12}$$

where the last equation is obtained from the linear approximation to the second equation in (1). Direct comparison between Eqs. (11) and (12) gives the relation between the mode shapes in the linear displacement/rotations along the beam axis and the modes in intrinsic variables, as

$$\begin{aligned} \boldsymbol{\Phi}_{1j} &\propto \omega_j \boldsymbol{\Phi}_{0j}, \\ \boldsymbol{\Phi}_{2j} &\propto \mathbf{c}^{-1} \left(\boldsymbol{\Phi}_{0j}' - \mathbf{e}^\top \boldsymbol{\Phi}_{0j}\right). \end{aligned} \tag{13}$$

where the proportionally constant is defined for each mode by the orthogonality conditions (6). As a result, all the coefficients in the nonlinear equations of motion in intrinsic coordinates, Eqs. (8), can be obtained from the structure natural frequencies, ω_j, and mode shapes, given in terms of displacement/rotation, $\boldsymbol{\Phi}_{0j}(s)$, and the (constant) cross-sectional mass and stiffness matrices, $\mathbf{m}$ and $\mathbf{c}$, respectively. Those will be calculated next.

D.   Integration in aeroelastic analysis

A process to integrate the equations of motion in intrinsic modal coordinates, Eqs. (8), into a full-vehicle nonlinear aeroelastic analysis is shown in Figure 1. The current displacements, $\mathbf{x}_0$, and velocities, $\mathbf{x}_1$, define the instantaneous boundary conditions for the time-domain aerodynamics. They can be a full-field solver (e.g., Euler, RANS) or a geometrically-nonlinear panel method (e.g., UVLM). If deformations were small, a frozen geometry can be assumed (i.e., constant $\mathbf{x}_0$), and the aerodynamics could also be obtained by the conventional linear methods (e.g., DLM). Also, if a strip model can be used for the aerodynamics, in which the local forces are given by some unsteady thin aerofoil theory, then only the beam velocities are needed to enforce the non-penetrating boundary conditions in the aerodynamic solution.[16, 24]

Integration of sectional aerodynamic loads produces the vector of resultant forces and moments, $\mathbf{f}_1$, which can be now projected on the modal space. The resultant modal forces, Q_1, are then applied on the structure. Since the modal equations of motion, Eqs. (8), are written in polynomial form, one can separate the linear and nonlinear contributions. This provides an avenue for the solution of the problem using the Increased-Order Modelling[25] approach. The beam velocities, $\mathbf{x}_1$, are obtained from the corresponding modal coordinates and

they are finally integrated in time. Note that Eq. (10) is only valid for the linear case, and in general this integration needs to be approached by the standard methods of rigid-body dynamics.[21] Alternative, the internal forces and moments, $\mathbf{x}_2$ can be used as the main output and the displacements/rotations are then obtained through spatial integration at each time step.[24]
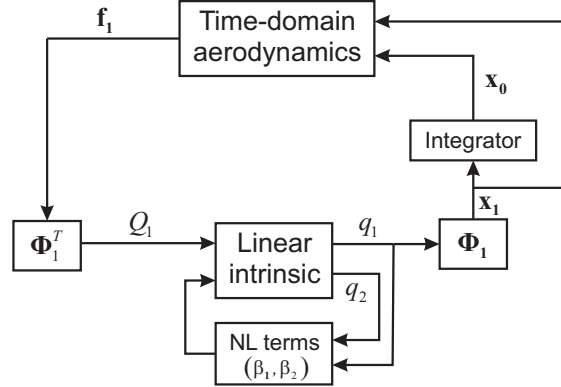

Figure 1: Flow diagram of nonlinear aeroelastic analysis with structural dynamics solved in intrinsic modal coordinates.

III.   Static condensation of the full 3-D model

We can now focus our attention to the detailed 3-D FEM model. As mentioned in the introduction, the assumption in this work is that a complex-geometry finite-element model has been built for the linear dynamic load and aeroelastic analysis of a full aircraft. The global mass, $\mathbf{M}_g$, and stiffness, $\mathbf{K}_g$, matrices of that model are computed by, say, Nastran, and are directly available. A *beam skeleton* is also defined on the full model that links the master nodes on which the structure will be reduced. Such nodes often exist in structural dynamics models to extract resultant dynamic loads. The master nodes are added to the original model and linked to the local structural nodes by means of an interpolation element (RBE3 in Nastran). A further simplification is obtained if masses are defined directly on the master nodes, as it is typically done for dynamic load analysis, although this is not strictly necessary. A Guyan reduction[18, 19] is now carried out on the full equations of motion using the degrees of freedom (three displacements and three rotations) at the master nodes as the reduced set. That results in reduced matrices $\mathbf{M}_a$ and $\mathbf{K}_a$, which, importantly, are full matrices. As it will be shown with the numerical examples, the slenderness of the structure brings, however, a block-diagonal structure into the reduced matrices. One can define a matrix of connectivities between master nodes, $\mathbf{T}$, with takes 1 on the terms corresponding to consecutive master nodes and zeros between nodes that are further apart. As the slenderness of the primary components on the actual structure increases, the terms outside the mapping $\mathbf{T} \bullet \mathbf{K}_a$ will go to zero (where $\bullet$ is the element-by-element matrix multiplication operator). In the limit in which all the nodes on the omitted set are infinitesimally closed to a node in the reduced set (infinite aspect ratio), then it will be $\mathbf{K}_a = \mathbf{T} \bullet \mathbf{K}_a$, that is, the reduced matrix corresponds to the actual beam model.

The reduction process into the nonlinear equations in intrinsic modal coordinates will proceed as follows:

1. Let $\boldsymbol{\phi}_{aj}$ be the discrete mode shapes in displacement/rotation degrees of freedom obtained in the reduced set (a-set), that is, from the solution of the eigenvalue problem

$$\left(-\omega_j^2 \mathbf{M}_a + \mathbf{K}_a\right) \boldsymbol{\phi}_{aj} = 0. \tag{14}$$

   This equation determines the natural frequencies, ω_j in Eq. (8), that is, the linear description of the intrinsic problem (8) is directly based on the results of the static condensation.

2. The coefficients for the nonlinear terms, given by Eq. (9), need the mode shapes in intrinsic variables and the distribution of mass and stiffness. The mode shapes in velocities, $\boldsymbol{\Phi}_{1j}$, are obtained directly

American Institute of Aeronautics and Astronautics

from the first of Eqs. (13) with the modes approximated by $\boldsymbol{\phi}_{aj}$. The mode shapes in internal forces/moments, $\boldsymbol{\Phi}_{2j}$ can also be obtained from the vibration analysis on the reduced model, using similar approaches to load analysis.[26] Two alternative methods can be considered:

(a) *The mode-displacement approach*: From the mode shapes in the reduced set, $\boldsymbol{\phi}_{aj}$, a static equilibrium can be computed (under displacement loads), that is,

$$\boldsymbol{f}_{aj}^{ext} = \mathbf{K}_a \boldsymbol{\phi}_{aj}. \tag{15}$$

Once the equivalent external forces are obtained, the internal forces at any given location are simply obtained by computing the resultant forces at any given section, as it is done in load analysis.[26]

(b) *A fictitious-mass approach*: Karpel and Presente[27] showed that the mode-displacement method may be inaccurate to compute wing sectional loads and proposed using a penalty method instead. It collocates three grid points (with 6 degrees of freedom each) at each master node of the reduced set: Two "outboard" points represents the edges of the beam segments that finish at that point, and a "middle" point is loaded by large fictitious mass matrix, M_f (such that $\|M_f\| \to \infty$), in all six degrees of freedom. Multi-point constraints now force the (dependent) middle-point displacements to be equal to the difference between the displacements of the respective inboard and outboard points. The fictitious masses do not effectively modified the LNMs modes of the original problem, but evaluation of their component at the dependent nodes yields directly the resultant forces at the node locations, s_f, as

$$\boldsymbol{\Phi}_{2j}(s_f) = \omega_j^2 M_f \phi_{aj}(s_f). \tag{16}$$

Equation (12) also provides important information about the normalization of the eigenvectors. If the velocity component to the mode shape, $\boldsymbol{\Phi}_{1j}$, is normalized according to the first of Eqs. (6), then the second equation will be satisfied automatically by the force component of the mode shape. As discussed above, this is an important property, since the mass matrix is diagonal in the a-set (that is $\mathbf{M}_a = \mathbf{T} \bullet \mathbf{M}_a$) and allows the direct evaluation of the sectional mass matrix, $\mathbf{m}$. This is not the case for the sectional compliance matrix, $\mathbf{c}$, which requires further attention. This is done next.

3. All terms in Eq. (8) have been already identified except for the compliance matrix, $\mathbf{c}$, which is required for the β_2 coefficients multiplying the quadratic terms in Eq. (9). Alternatively, the products $\mathbf{c}\boldsymbol{\Phi}_{2j}$ could be directly obtained. Several possible alternatives have been explored here:

(a) A first approach, that was already outline above, is the direct identification of terms in $\mathbf{T} \bullet \mathbf{K}_a$ with those that would be obtained using linear beam elements between the nodes in the reduced set. The stiffness on each equivalent beam element would be

$$\mathbf{K}_e = \int_0^{L_e} \mathcal{B}^\top \mathbf{c}^{-1} \mathcal{B} ds \tag{17}$$

where $\mathcal{B}$ is the strain matrix in the linear 2-noded beam element of length L_e. Comparing $\mathbf{K}_e$ with the corresponding sub-block in the reduced stiffness $\mathbf{K}_a$, one can estimate the value of the constants in the compliance matrix $\mathbf{c}$. Note that this, in particular, imposes no restrictions to $\mathbf{c}$, that can be a full matrix. Finally, the relative values of the terms that are discarded in this process serve to estimate the validity of the beam approximation. As it will be seen through numerical examples, this approach only works well in practice for very-high-aspect-ratio beam elements.

(b) An alternative method is obtained by directly obtaining the products $\mathbf{c}\boldsymbol{\Phi}_{2j}$, that is, the equivalent beam strains associated to each mode, since from Eq. (13) they can be obtained directly from the local derivatives of the mode shapes in displacements.

(c) A third method, valid only for constant section beams, is possible by using the second of the orthogonality conditions defined in Eq. (6) with the known mode shapes.

All these different approaches would give the same outcome in the limit of beams with infinite aspect ratio, but each of them approaches differently the estimation of the equivalent stiffness for structures of finite cross-sectional dimensions. Their relative performance will be investigated through numerical examples in the next section.

American Institute of Aeronautics and Astronautics

IV.   A Numerical Example

The previous procedure will be exemplified on a simple prismatic thin-walled cantilever with constant isotropic properties ($E = 10^6$, $\nu = 0.3$, $\rho = 1$). The box beam has length L, width w, height h, and walls of thickness t (with $t << w, h$). In this case, an assuming a large aspect ratio of the beam ($L >> w, h$), there is an analytical solution to the problem that can be used as reference. Finite-element models have also been built using shell elements, such as the one shown in Figure 2. In all the results that follow it was $t=0.01$, $w=1$.
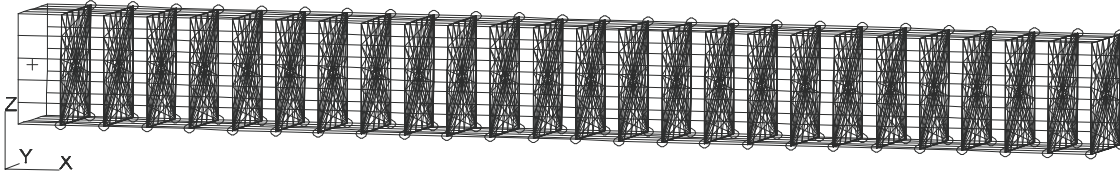
Figure 2: FEM model for $L = 10$ and $h = 1$, showing rigid links (RBE3) to interpolate sectional displacements/rotations on nodes along centre line.

A.   Solution for constant cross-sections

The analytical solution of the intrinsic beam problem with constant cross-section is presented first. The relevant sectional constants in this problem are those of Euler-Bernoulli beam, that is,

$$
\begin{aligned}
\mathbf{m} &= diag\left\{\rho A, \rho A, \rho A, \rho I_1, 0, 0\right\}, \\
\mathbf{c}^{-1} &= diag\left\{EA, 0, 0, GJ, EI_2, EI_3\right\}.
\end{aligned}
\tag{18}
$$

Its LNMs in intrinsic degrees of freedom can be now obtained.[16]

1.   Axial and torsional modes

The eigenvalues of the axial problem are $\omega_j = \sqrt{\frac{E}{\rho}}\lambda_j$, with $\lambda_j = \frac{2j-1}{2}\frac{\pi}{L}$ and $j = 0, 1, 2, ..., \infty$. The corresponding eigenvectors, after normalization, are

$$
\begin{aligned}
\Phi_{V_1 j} &= \sqrt{\frac{2}{\rho A L}}\sin\left(\lambda_j s\right), \\
\Phi_{F_1 j} &= -\sqrt{\frac{2EA}{L}}\cos\left(\lambda_j s\right).
\end{aligned}
\tag{19}
$$

The same results are obtain for the torsional modes, with GJ replacing EA and I_1 instead of A.

2.   Bending modes

The natural frequencies in the x-z plane are $\omega_j = (\lambda_j)^2\sqrt{\frac{EI_2}{\rho A}}$, where λ_j are the solutions to the well-known equation,

$$
\cos(\lambda_j L)\cosh(\lambda_j L) + 1 = 0.
\tag{20}
$$

American Institute of Aeronautics and Astronautics

The corresponding eigenvectors are

$$\Phi_{V3j} = \frac{1}{\sqrt{\rho AL}} \left[\cos(\lambda_j s) - \cosh(\lambda_j s) - \Lambda_j(\sin(\lambda_j s) - \sinh(\lambda_j s)) \right],$$

$$\Phi_{\Omega 2j} = \frac{\lambda_j}{\sqrt{\rho AL}} \left[\sin(\lambda_j s) + \sinh(\lambda_j s) + \Lambda_j(\cos(\lambda_j s) - \cosh(\lambda_j s)) \right],$$

$$\Phi_{F3j} = \lambda_j \sqrt{\frac{EI_2}{L}} \left[\sin(\lambda_j s) - \sinh(\lambda_j s) + \Lambda_j(\cos(\lambda_j s) + \cosh(\lambda_j s)) \right], \tag{21}$$

$$\Phi_{M2j} = \sqrt{\frac{EI_2}{L}} \left[-\cos(\lambda_j s) - \cosh(\lambda_j s) + \Lambda_j(\sin(\lambda_j s) + \sinh(\lambda_j s)) \right],$$

with

$$\Lambda_j = \frac{\cos(\lambda_j L) + \cosh(\lambda_j L)}{\sin(\lambda_j L) + \sinh(\lambda_j L)}. \tag{22}$$

These functions can be now used to obtain the coefficients in the modal equations of motion, Eqs. (8).

B.   Evaluation of coefficients from 3-D problem

Models for the reference box beam are built using 4-noded shell elements in MD Nastran (v2012.1.0). The discretization for $L=10$ and $h=1$ is shown in Figure 2. The figure includes the connections between nodes at each spanwise location and the master nodes (25 in total) along the beam axis where displacements are interpolated. Masses are lumped on the master nodes.
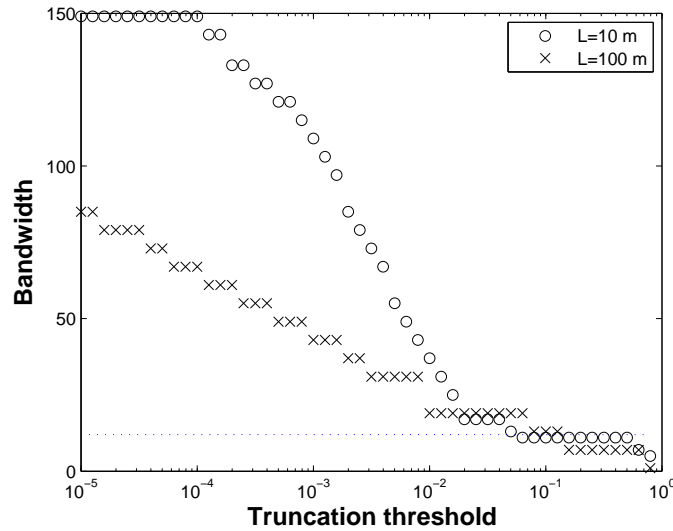

Figure 3: Bandwidth of the truncated reduced stiffness matrix vs. truncation threshold for the prismatic bar. The dotted line marks the bandwidth of the corresponding beam model [$h=1$ and two beam lengths].

The reduced mass matrix, $\mathbf{M}_a$, is thus diagonal. We first investigate the bandwidth on the reduced stiffness matrix, $\mathbf{K}_a$. This is shown in Figure 3 for $h=1$ and for two different beam lengths, $L=10$ and 100. This bandwidth is determined after terms below a given truncation threshold are cancelled. The truncation is defined through comparison of the absolute value of coupling terms in the matrix with the corresponding coefficients in the diagonal. The size of the reduced matrix in this problem is 150 and it has non-zero terms in all its coefficients. As one can see in Figure 3, however, the off-diagonal terms have small magnitude and, as the threshold increases the bandwidth of the resulting matrix rapidly reduces. The dotted line in the figure shows the maximum half-bandwidth (that is, 12) of a model made of beam elements that would connect the master nodes. Thus, for a very slender beam ($L=100$), a beam-like stiffness matrix is obtained by truncating off-diagonal terms smaller than 5%, while for $L=10$ the required truncation increases to 15%.

American Institute of Aeronautics and Astronautics

This metric gives a good estimation of the error associated to modelling the actual structure using beam elements.

The linear coefficients in Eqs. (8) (that is, the natural frequencies –and the corresponding mode shapes–) can be obtained directly from the model obtained from Guyan reduction, as in standard aeroelastic analysis. The nonlinear terms, defined by Eqs. (9) depend on the mode shapes at the master nodes, which are also obtained from the reduced model, with results post-processed with Eq. (13), and the identification of the sectional stiffness coefficients in the truncated reduced stiffness matrix of the problem. The reduced mass matrix is diagonal since the masses have been already concentrated at the master nodes. In this example, only the axial and torsional terms have been obtained.

(a) Axial Stiffness　　　　　　　　　　　(b) Torsional Stiffness
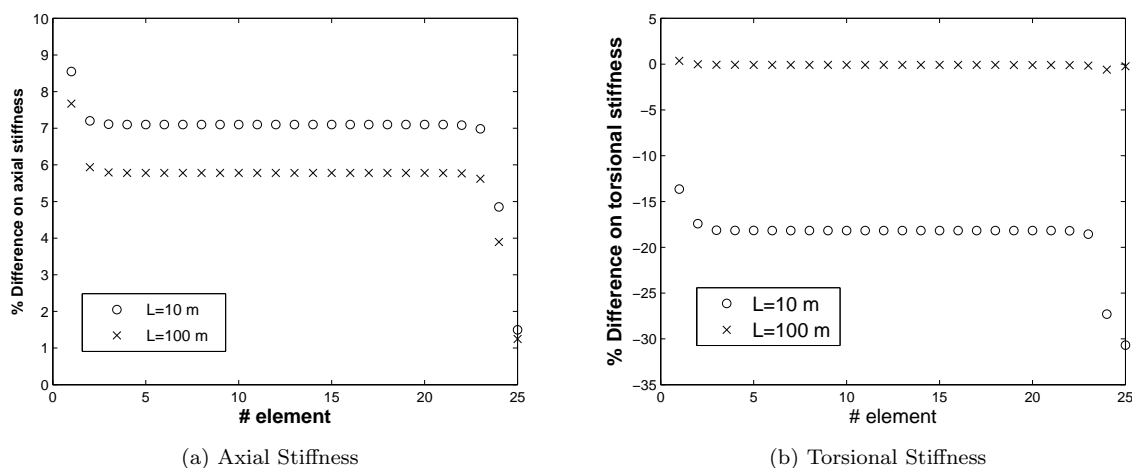
Figure 4: Difference between the beam stiffness constants obtained from $\boldsymbol{K_a}$ and the constant-section solution for a thin-wall beam [h=1].

For this simple geometry, the analytical results introduced above allow a direct evaluation of the approximation obtained by the present method. This comparison is carried out in Figure 4 for the axial (EA) and torsion (GJ) coefficients obtained for the prismatic bars under consideration. The numerical results in the figure are normalized with the constant-section expressions. Tesults get closer to the analytical expressions as the length of the beam increases, but it is obvious that the direct identification of sectional stiffness in $\mathbf{K}_a$ does not produce satisfactory results. The biggest difference appears for the torsional coefficient for the shorter beam (L =10) where the difference outside the beam boundaries is about 18%. This number is consistent with the truncation threshold of the reduced stiffness matrix matrix (which was established above at 15%) that gave a metric of the error introduced when obtaining a beam model from the actual structure. For the case with extremely large aspect ratio, the comparison is excellent, which confirms that in the limit $L \to \infty$, the stifness matrix $\mathbf{K}_a$ is indeed a block diagonal matrix. After this preliminary investigation, the next sections will compute the different coefficients on the nonlinear equations of motion for this box beam configuration.

1. *Natural frequencies and mode shapes*

The natural frequencies were first obtained for a geometry defined by L=20 and varying cross-sectional height, h. They are selected such that their eigenvectors span the whole space of possible nonlinear deformations. Therefore, the first few modes in bending, twisting and axial deformations are included, even when they are at very high frequencies. The list of relevant modes here is is listed in Table 1 for h=0.01 and h=0.05, and it includes the number in which they appear in the reduced-set solution of the FEM model. The first three out-of-plane bending mode shapes, in intrinsic coordinates (i.e., velocities and internal forces) are shown in Figure 5 for h=0.01. Results compare the modes on the reduced problem with those obtained from the constant-section beam solution and the modes are normalized as in Eq. (6). As it was mentioned above, there is no need to know the sectional compliance matrix, $\mathbf{c}$, to normalize the component of the modes in internal forces/moments $\boldsymbol{\Phi}_2$, since they are obtained from the same set of modes in displacements, $\boldsymbol{\Phi}_0$, as

American Institute of Aeronautics and Astronautics

the modes in velocities, $\mathbf{\Phi}_1$. The comparison between both sets of modes is excellent.

Table 1: Natural angular frequencies after static condensation in the 3-D FEM. N_{FEM} is the mode number in the FEM model. They are compared with Euler-Bernoulli beam results [L=20].

Mode type	h=0.1			h=0.5		
	N_{FEM}	ω_{beam}	ω_{FEM}	N_{FEM}	ω_{beam}	ω_{FEM}
1st x-z bending	1	0.426	0.411	1	1.94	1.86
2nd x-z bending	2	2.67	2.56	3	12.15	11.43
3rd x-z bending	4	7.47	7.11	6	34.01	29.92
1st x-y bending	3	2.76	2.65	2	3.28	3.15
2nd x-y bending	7	17.29	16.51	4	20.53	19.32
3rd x-y bending	13	48.41	45.70	9	57.48	51.29
1st torsion	5	13.95	13.33	5	37.50	29.50
2nd torsion	10	41.83	32.94	7	112.49	45.48
1st axial	21	78.54	77.07	13	78.54	77.08
2nd axial	47	235.62	230.78	58	235.62	230.78

A comparison of the first two axial and torsional mode shapes for that same geometry is shown in Figure 6. The comparison with the axial modes is also excellent. Note from Table 1 that the second mode is a very high frequency mode, but it is retained to provide a basis for capturing in-plane deformations in the nonlinear beam dynamics. As one would expect, only the first torsional mode is approximately captured by the Euler-Bernoulli beam model; the natural angular frequency of the second torsional is substantially over-predicted by this analytical model. Indeed, end effects become significant for shorter wavelengths and require 1-D solutions that include warping restriction methods. It is important to emphasize however that the constant-section beam solution is included here only as a reference, since for this simple geometry that solution is readily available. The nonlinear model here will be directly based on the results from the 3-D FEM and those are the frequencies and mode shapes that will be used. In other words, the present method, being based on an actual built-up geometrically-accurate model of the structure, naturally includes end effects due to kinematic restrictions on the real geometry.

Once the modes in intrinsic coordinates, $\mathbf{\Phi}_j$, and their angular frequencies, ω_j, and the sectional mass matrix $\mathbf{m}$ have been obtained, the average sectional stiffness matrix can be obtained from the second Eq. (6). This can be obtained from all ten modes in Table 1 by means of a least squares solution. To obtain the coefficients of beam theory, however, it is better to limit the minimum number of them (the first two bending modes in each axis, and the first axial and torsion modes). Results for the same case as before, that is, L=20, w=1, h=0.1, t=0.01, give a diagonal matrix within the accuracy of the problem, which can be compared to the analytical expressions from beam theory. The coefficients are (with beam theory constants in parenthesis) $EA = 2.21 \times 10^5$ (2.22×10^5); GJ=66.9 (69.9), EI_3=56.2 (51.7), and $EI_2 = 2.35 \times 10^3$ (2.17×10^3). The comparison between both cases is acceptable, but it is less satisfactory than the one on reduced frequencies in Table 1. However, the assumption of constant stiffness is indeed not needed. In fact, as it was mentioned in section III, the compliance matrix is actually not directly needed, and we only need to compute the product $\mathbf{c}\mathbf{\Phi}_{2j}$ for each mode shape. This physically represents the force and moment strains (curvatures) of the modes. The curvatures for the first out-of-plane bending and torsional modes, obtained from a finite-difference approximation to the second of Eqs. (13), are shown in Figure 7. Results are compared against the constant-section beam solutions. As before, bending mode compare well, while restrained warping on torsional modes is not included in the beam model and creates significant differences at both ends in Figure 7a, which increase with the mode shapes. Note that the beam solution is the approximation to the solution from 3-D FEM and not the other way around. At this stage, we can obtain all the coefficients of equations of motion in intrinsic modal coordinates, Eqs. (8), directly from linear 3-D finite-element analysis.
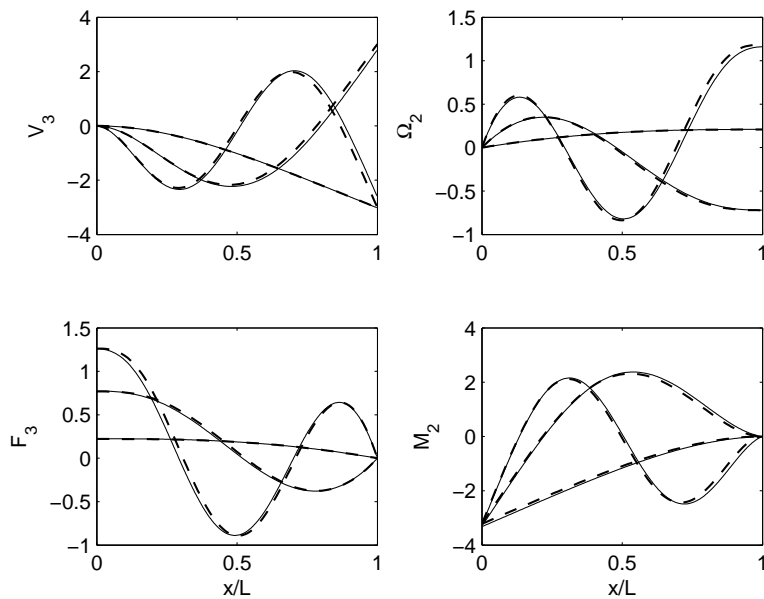
Figure 5: Out-of-plane bending modes in intrinsic coordinates from the reduction from 3-D FEM (continuous lines) and the constant-section beam model (dashed) [L=20, h=0.1].
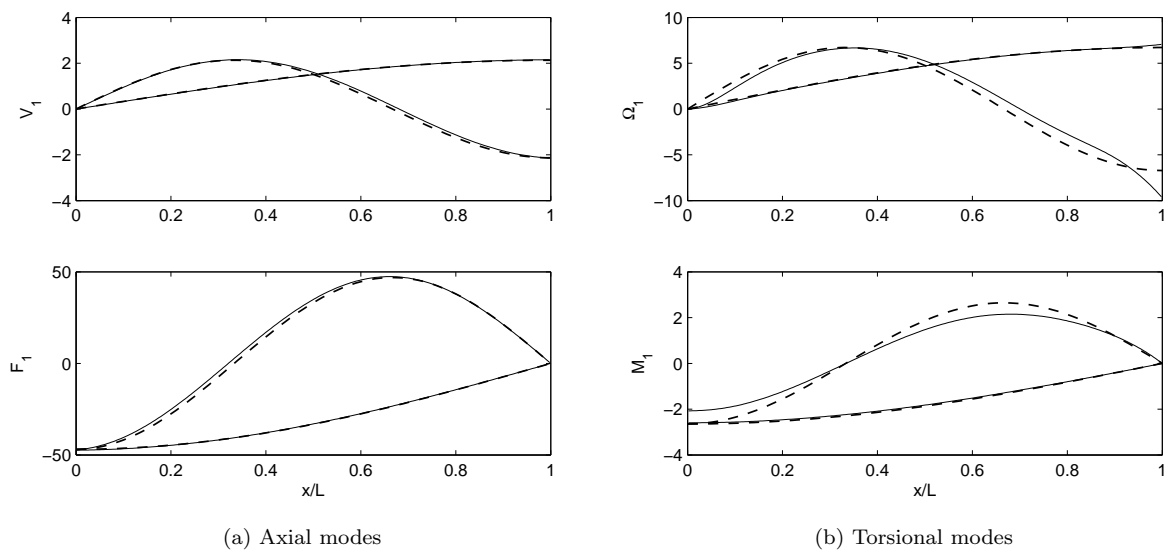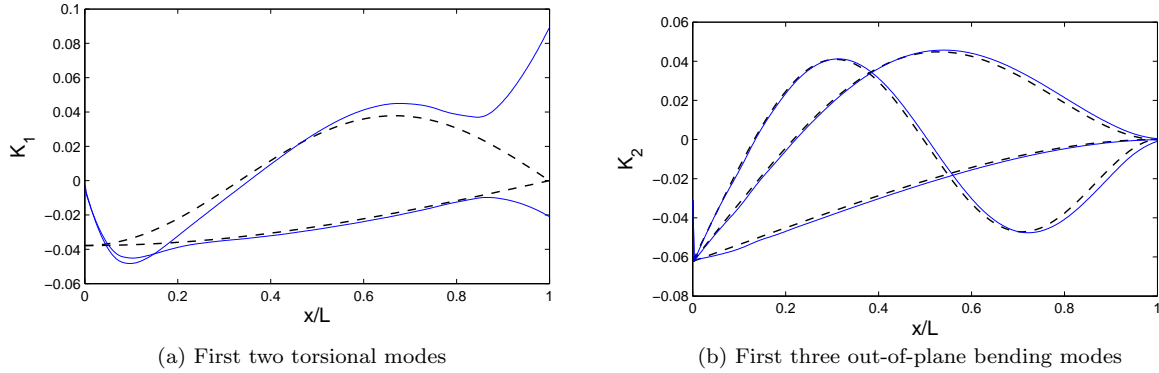

(a) Axial modes

(b) Torsional modes

Figure 6: First two axial and torsional modes in intrinsic coordinates from the reduction from 3-D FEM (continuous lines) and the constant-section beam model (dashed) [L=20, h=0.1].

American Institute of Aeronautics and Astronautics

(a) First two torsional modes

(b) First three out-of-plane bending modes

Figure 7: Curvature of the mode shapes, $\mathbf{c}\boldsymbol{\Phi}_{2j}$, as obtained from 3-D FEM (continuous lines) and the constant-section beam model (dashed) [L=20, h=0.1].

C. Geometrically-nonlinear beam dynamics

Once the coefficients for the geometrically-nonlinear equations of motion have been identified, the beam dynamics can be investigated. The geometry in this section is again defined as L=20, w=1, h=0.1, and t=0.01, for which all mode shapes in intrinsic variables were shown in the previous section. The simulations correspond to free vibrations for a parabolic initial velocity distribution, given as $x_1(s,0) = x_{10}(\frac{s}{L})^2$, where x_{10} will be the parameter in the different test cases. An explicit 4th-order Runge-Kutta was used to solve the implicit equations (8) with a time step Δt=0.02 and no structural damping. Translational/angular velocities and internal forces/moments are then obtained using the modal expansions in Eq. (7). Finally, as shown in Figure 1, the material velocities are integrated at the point of interest using the equations of rigid body dynamics.

Figure 8 shows the velocities and displacements at the free end of the box beam for small initial velocities, $x_{10} = (0, 0.002, 0.002, 0, 0, 0)$. In this case, the response is in the linear regime and can be compared directly with that obtained from Nastran after the static condensation. The intrinsic solution is based on the 10 modes shown in Table 1. As the modes in the intrinsic method are directly obtain from the 3-D model, the comparison is excellent. The small differences are simply due to the modal truncation in the intrinsic solution.

As the amplitude of the initial velocities increases, geometrically-nonlinear become more important. Figure 9 shows the displacements and velocities at the free end, $s = L$, with $x_{10} = (0, 2, 2, 0, 0, 0)$. Maximum tip displacements in this case are about 25% of the beam length. The first thing to observe is that we need a larger modal basis to obtain converged results. Figure 9 compares the results obtained using the 10 (selected) modes used for the linear case, which were sufficient for that problem, the first 18 modes plus the first two axial modes in Table 1 (N =20) and the first 50 modes of the reduced set on the 3-D FEM. The shift in the frequency of the in-plane motions would not be capture with on the small modal basis. The bigger basis is not needed because there are higher frequencies present in the response, but mostly because of the additional mode shapes are needed to approximate the instantaneous deformed shapes in the nonlinear response. In particular, as it has been already shown,[17] if no axial modes were included, there would be no couplings in the deformations on the beam principal bending planes. As it can be seen from Figure 9, results have converged for the case N =20. This is further investigated in Figure 10, which shows the time history of the first 20 modal amplitudes (force component, q_2) for the same geometry and initial conditions. Modes 1-10 are in black and the rest in blue and all visible modes in table 1 are included. Note that the torsional modes, which are not excited in the linear case, are rather significant and their amplitude is essentially modulated by the first bending mode in each plane. This finite-rotation effect occurs when there is simultaneous bending in both axis and disappears for planar deformations.

It is interesting to compare those results with those that would be obtained with bending motions in only one plane. Figure 11 shows the tip displacements and the modal amplitudes for initial conditions in the x-z plane. The displacement values show results for small and large initial velocities and a comparison between the present method and those obtained by the constant-section beam models (both using an in-
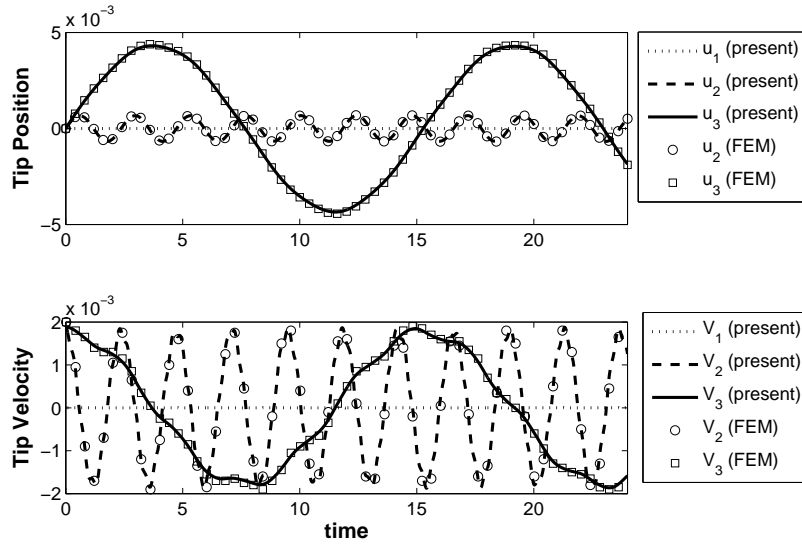
Figure 8: Displacements and velocities at $s = L$ for small initial velocities. Results from Nastran and the present method. $[x_{10} = (0, 0.002, 0.002, 0, 0, 0)]$.

(a) Displacements (in global coordinates)
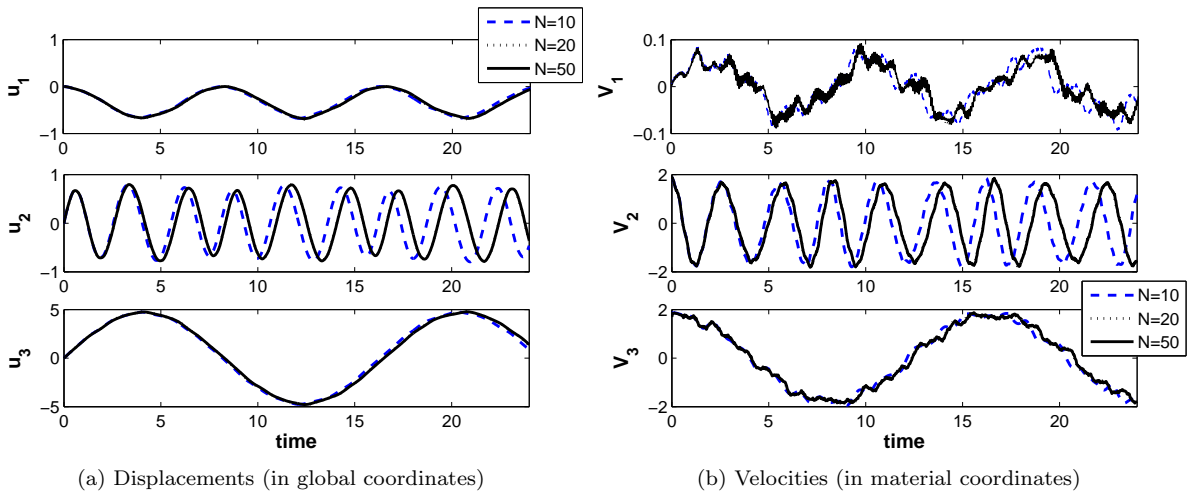
(b) Velocities (in material coordinates)

Figure 9: Displacements and velocities at $s = L$ for large initial velocities, $x_{10} = (0, 2, 2, 0, 0, 0)$, and increasing number of LNMs in the nonlinear intrinsic model.
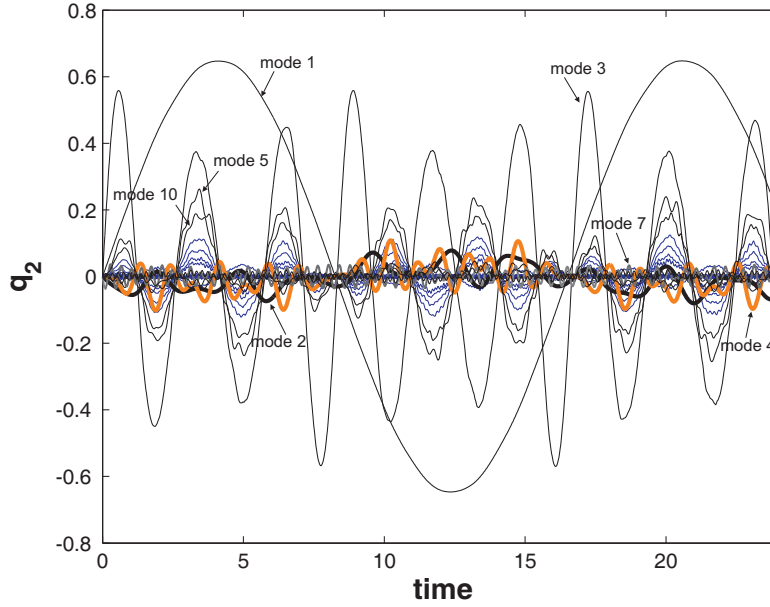
Figure 10:   First 20 modal amplitudes of the force component q_2 and initial conditions $x_{10} = (0, 2, 2, 0, 0, 0)$. Modes 1-10 in black and modes 11-20 in blue. All visible modes from Table 1 have been identified.

trinsic description and a standard FE solution). Since the constant-section models overestimate the natural frequencies, there is a small difference in the results, but the agreement is very good beyond that change on the period of the oscillations. The modal components are more interesting and show that only the first two bending modes and the first axial mode (mode 21 in Table 1) are excited. Similar results would be obtained for the motions in the x-y, and, of course, none of them show the coupling with the torsional modes that appears when the initial condition includes *both* bending components, as it was seen in Figure 10.

Finally, Figure 12 compares the previous converged results (with 50 LNMs) for initial conditions $x_{10} = (0, 2, 2, 0, 0, 0)$ (motion in both planes) with those obtained from the constant-section beam equations. Those equations were solved using an intrinsic description (with, as before, the LNMs defined as in section IV.A) and through standard finite-elements based on nodal displacements and rotations. The finite-element solution is a converged geometrically-nonlinear solution using 200 B31 elements in Abaqus with a time step $\Delta t = 0.01$. Very good agreement can be observed between both beam models, which may serve to validate our implementation of the nonlinear intrinsic beam solver, but, as before, more significant differences are seen when the coefficients in the intrinsic equations are obtained from the reduced model. They are mostly due to the different frequencies of the LNMs, but they are also magnified here by the relatively poor approximation to the torsional modes in the constant-section models. As it was discussed above, the constant-section beam should be considered only as a first approximation to the results based on 3-D information obtained by the present method.

V.   Conclusions

The paper has shown a procedure to obtain compact geometrically-nonlinear descriptions from the detailed 3-D finite-element models used for full-vehicle aeroelastic and load analysis. The condition for this is that the static condensation in the structural model is carried out into grid nodes along a virtual *beam skeleton* of the original structure. This is in fact just exploiting the usual approach to obtain "interesting quantities" in load analysis, but it does not preclude the possibility of branches that link the spanwise reference line to, for instance, ailerons or engines.

The formulation is modal and it uses directly the linear normal modes of the reduced structure. As a result, there is no loss of accuracy in linear analysis beyond that of the Guyan condensation. It is intrinsic,
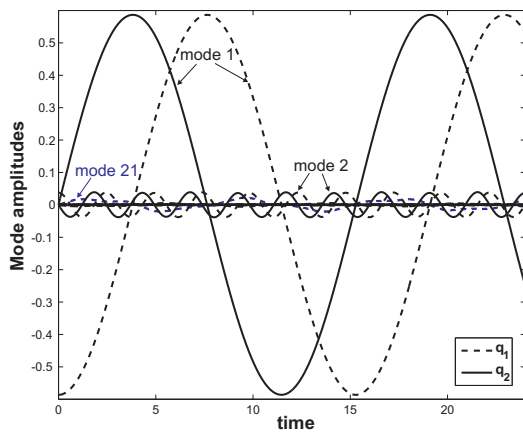
(a) Modal amplitudes for the modes in Table 1. All visible modes have been identified. $x_{10} = (0, 0, 2, 0, 0, 0)$
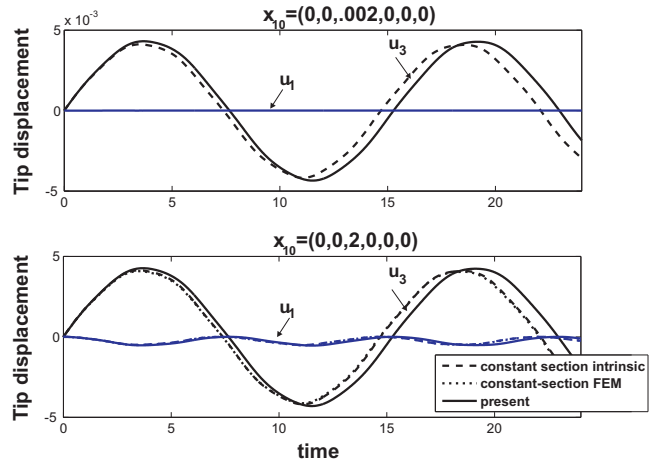
(b) Displacements (in global coordinates)

Figure 11: Modal amplitudes and displacements at $s = L$ for motions in the $x - z$ plane.
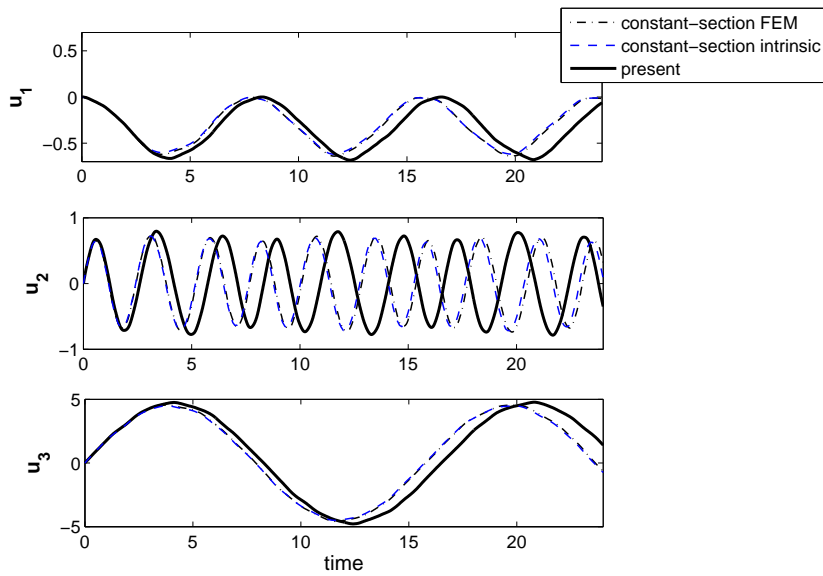

Figure 12: Components of the displacements (in the global frame) at $s = L$ for large initial velocities $[x_{10} = (0, 2, 2, 0, 0, 0)]$.

American Institute of Aeronautics and Astronautics

which means that it transforms the mode shapes from displacements into their spatial derivatives (strains, or internal forces) and time derivatives (velocities). We show however how this does present major obstacles in the integration into a standard time-domain nonlinear aeroelastic analysis. Indeed in the limit to small deformations it converges to standard linear aeroelastic analysis, what allows tackling the problem using an Increased-Order-Model approach.

Numerical results have been presented for a cantilever box beam. It is first shown that the nonlinear equations of motion can be built directly from the shell model and it has identified that the best method to obtain the nonlinear coefficients is probably the direct computation of curvatures for each mode, which removes the estimation of the sectional compliance matrix. Results were presented against nonlinear beam models and showed the relatively-large impact that the improved description in capturing the torsional modes and the corresponding couplings that apppear 3-D nonlinear beam dynamics.

Acknowledgements

References

[1]Drela, M., "Integrated simulation model for preliminary aerodynamic, structural, and control-law design of aircraft," *40th AIAA/ASME/ASCE/AHS/ASC Structures, Structural Dynamics and Materials Conference, St. Louis, Missouri, USA. AIAA Paper 1999-1394*, April 1999.

[2]Patil, M. J., Hodges, D., and Cesnik, C., "Nonlinear Aeroelastic Analysis of Complete Aircraft in Subsonic Flow," *Journal of Aircraft*, Vol. 37, No. 5, 2000, pp. 753–760.

[3]Patil, M. J. and Hodges, D., "Flight Dynamics of Highly Flexible Flying Wings," *Journal of Aircraft*, Vol. 43, No. 6, 2006, pp. 1790–1798.

[4]Shearer, C. and Cesnik, C., "Nonlinear Flight Dynamics of Very Flexible Aircraft," *Journal of Aircraft*, Vol. 44, No. 5, 2007, pp. 1528–1545.

[5]Su, W. and Cesnik, C., "Nonlinear Aeroelasticity of a Very Flexible Blended-Wing-Body Aircraft," *Journal of Aircraft*, Vol. 47, No. 5, 2010, pp. 1539–1553.

[6]Murua, J., Palacios, R., and Graham, J., "Applications of the unsteady vortex-lattice method in aircraft aeroelasticity and flight dynamics," *Progress in Aerospace Sciences*, 2012, To Appear.

[7]Wang, Z., Chen, P. C., Liu, D. D., and Mook, D. T., "Nonlinear-Aerodynamics/Nonlinear-Structure Interaction Methodology for a High-Altitude Long-Endurance Wing," *Journal of Aircraft*, Vol. 47, No. 2, 2010, pp. 556–566.

[8]Murua, J., Hesse, H., Palacios, R., and Graham, J., "Stability and Open-Loop Dynamics of Very Flexible Aircraft Including Free-Wake Effects," *52nd AIAA/ASME/ASCE/AHS/ASC Structures, Structural Dynamics and Materials Conference, Denver, Colorado, USA*, April 2011.

[9]Murua, J., Palacios, R., and Graham, J., "A discrete-time state-space model with wake interference for stability analysis of flexible aircraft," *15th International Forum of Aeroelasticity and Structural Dynamics*, Paris, France, June 2011.

[10]Cesnik, C. and Hodges, D., "VABS: A New Concept for Composite Rotor Blade Cross-Sectional Modeling," *Journal of the American Helicopter Society*, Vol. 42, No. 1, 1997, pp. 27–38.

[11]Lee, C. and Yu, W., "Variational Asymptotic Modeling of Composite Beams with Spanwise Heterogeneity," *52nd AIAA/ASME/ASCE/AHS/ASC Structures, Structural Dynamics and Materials Conference, Denver, Colorado, USA*, No. 2011-1851, April 2011.

[12]Elsayed, M., Sedaghati, R., and Abdo, M., "Accurate Stick Model Development for Static Analysis of Complex Aircraft Wing-Box Structures," *AIAA Journal*, Vol. 47, No. 9, September 2009, pp. 2063–2075.

[13]Hegemier, G. and Nair, S., "A Nonlinear Dynamical Theory for Heterogeneous, Anisotropic, Elastic Rods," *AIAA Journal*, Vol. 15, No. 1, 1977, pp. 8–15.

[14]Hodges, D., "Geometrically exact, intrinsic theory for dynamics of curved and twisted anisotropic beams," *AIAA Journal*, Vol. 41, No. 6, 2003, pp. 1131–7.

[15]Love, A. E. H., *A Treatise on the Mathematical Theory of Elasticity*, Dover Publications Inc, New York, NY, USA, 4th ed., 1944, (First published in 1927 by Cambridge University Press).

[16]Palacios, R. and Epureanu, B., "An Intrinsic Description of the Nonlinear Aeroelasticity of Very Flexible Wings," *52nd AIAA/ASME/ASCE/AHS/ASC Structures, Structural Dynamics and Materials Conference, Denver, Colorado, USA*, No. 2011-1917, April 2011.

[17]Palacios, R., "Nonlinear normal modes in an intrinsic theory of anisotropic beams," *Journal of Sound and Vibration*, Vol. 330, No. 8, April 2011, pp. 1772–1792.

[18]Guyan, R., "Reduction of Stiffness and Mass Matrices," *AIAA Journal*, Vol. 3, No. 2, Feb. 1965, pp. 380.

[19]Schaeffer, H., *MSC/NASTRAN Primer: Static and Normal Modes Analysis*, MSC. Software Corporation, Santa Ana, California, USA, 2nd ed., 2001.

[20]Bonisoli, E., Delprete, C., and Rosso, C., "Proposal of a modal-geometrical-based master nodes selection criterion in modal analysis," *Mechanical Systems and Signal Processing*, Vol. 23, No. 3, 2009, pp. 606 – 620.

[21]Stevens, B. L. and Lewis, F. L., *Aircraft Control and Simulation*, John Wiley & Sons, Inc., New York, NY, USA, 1992.

[22]Chang, C.-S., Hodges, D. H., and Patil, M. J., "Flight dynamics of highly flexible aircraft," *Journal of Aircraft*, Vol. 45, No. 2, 2008, pp. 538–545.

[23]Palacios, R., Murua, J., and Cook, R., "Structural and Aerodynamic Models in the Nonlinear Flight Dynamics of Very Flexible Aircraft," *AIAA Journal*, Vol. 48, No. 11, Nov. 2010, pp. 2648–2659.

[24]Sotoudeh, Z., Hodges, D., and Chang, C.-S., "Validation Studies for Aeroelastic Trim and Stability Analysis of Highly Flexible Aircraft," *Journal of Aircraft*, Vol. 47, No. 4, 2010, pp. 1240–1247.

[25]Karpel, M., "Increased-Order Modeling Framework for Nonlinear Aeroservoelastic Analysis," *15th International Forum of Aeroelasticity and Structural Dynamics*, Paris, France, June 2011.

[26]Karpel, M., Moulin, B., Presente, E., Anguita, L., Maderuelo, C., and Climent, H., "Dynamic Gust Loads Analysis for Transport Aircraft with Nonlinear Control Effects," *49th AIAA/ASME/ASCE/AHS/ASC Structures, Structural Dynamics, and Materials*, Schaumburg, Illinois, USA, April 2008, AIAA Paper 2008-1994.

[27]Karpel, M. and Presente, E., "Structural Dynamics Loads in Response to Impulsive Excitation," *Journal of Aircraft*, Vol. 32, No. 4, 1995, pp. 853–861.